CFD simulation of the liquid metal flow in high power laser welding of aluminum with electromagnetic weld pool support

Marcel Bachmann, Vjaceslav Avilov, Andrey Gumenyuk and Michael Rethmeier

***Abstract* —** The influence of an alternating current (ac) magnetic field during laser keyhole welding on the velocity, pressure and temperature field of a 20 mm thick non-ferromagnetic aluminum plate was investigated using a three-dimensional self-consistent laminar steady state numerical model. The finite element software (FEM) COMSOL Multiphysics was used to calculate the three-dimensional heat transfer, fluid dynamics and electromagnetic field partial differential equations iteratively. Major important physical effects of the laser welding process were taken into account: Thermocapillary (Marangoni) convection at the weld pool surfaces, natural convection due to gravity and latent heat of solid-liquid phase transition. The Carman-Kozeny equation was used to account for porous media morphology. It is shown that the gravity drop-out associated with welding of thick plate due to the hydrostatic pressure can be prevented by the application of an ac magnetic field, which forms a magnetic pressure that compensates for gravitational effects. The application of oscillating magnetic fields of up to 100 mT was investigated to allow for single-pass laser welding of thick aluminum plates. Hereby, the flow pattern in the molten zone and thus also the temperature distributions are significantly changed.

***Keywords*—**electromagnetic weld pool support, laser welding, Lorentz force, Marangoni stresses, natural convection

I. INTRODUCTION

IN the last years, laser deep penetration welding became a widely applied tool in a variety of industrial applications due to the available laser power of 20 kW and above for modern fiber laser allowing for single-pass welding of steel plates of up to 20 mm [1].

Using high-power laser enables for the so-called keyhole-mode welding. Hereby, a small amount of the metal vaporizes and builds a vertical cavity in the plate. The surrounding liquid metal which is accelerated at the surface of the weld pool due to the temperature-dependence of the surface tension flows around this cavity [2], [3].

When welding in the single-pass technique, that means joining two parts in only one single cycle, liquid metal tends to drop out of the weld bead due to the hydrostatic pressure which, above a critical limit, cannot be balanced by the surface tension forces. This paper describes a numerical fluid dynamics investigation on the topic of electromagnetically-assisted laser welding of aluminum to gain an insight into the phenomena happening hereby. Doing a computational fluid dynamics (CFD) simulation coupled with electromagnetic fields offers insights into the process that are difficult or hardly ever possible to be obtained experimentally. Published work in the field of computational laser welding research can be found in [4] – [6], e.g.

In contrast to the electron beam welding, primary the evolution of the modern laser sources allowed for a electromagnetic manipulation of the hydrodynamics in the pool of liquid metal. Generally, magnetohydrodynamics (MHD) describes the fluid flow of an electrically conducting media in presence of an electromagnetic field [7]. Theoretical principles of the working mechanisms of conducting fluids under electromagnetic conditions can be found in [8].

Electromagnetic-assisted laser welding experiments using high-frequency alternating magnetic fields as investigated in this paper can also be found in the literature (cf. [9], [10]). There, the principal applicability of such an electromagnetic weld support system as well as the great potential for single-pass laser welding applications are shown.

In this paper, the application of a high-frequent alternating magnetic field was applied to a keyhole mode full-penetration single-pass welding process of a 20 mm thick aluminum plate. The stabilization of the fluid flow behavior and the compensation of the hydrostatic pressure are reached by Lorentz forces in the weld pool, which was numerically investigated. The CFD model takes into account liquid metal flow, heat transfer and ac electromagnetic fields.

II. MATHEMATICAL MODELING

A. Assumptions & Simplifications

For the simulations that were conducted to obtain the flow field, the pressure distribution as well as the solution of the Maxwell equations for the electromagnetic field, it is necessary to simplify the problem to the most important physics. To be able to numerically handle the simulation model, it is concentrated here on the main aspects of the welding process simulation with incorporated electromagnetic field simulation. These are Marangoni stresses, natural convection, and solid-liquid phase change modeling on the

Manuscript received May 31, 2011.
Marcel Bachmann is with the BAM Federal Institute for Materials Research and Testing, Unter den Eichen 87, 12205 Berlin, Germany,
phone: +49 30 8104 2756; e-mail: marcel.bachmann@ bam.de)

hydrodynamic side, and a harmonic excitation of the magnetic field on the electromagnetic side.

Basic assumptions for the simulation are as follows:

- Steady state simulation.
- The geometry of the keyhole as well as the weld pool surfaces are fixed.
- Laminar flow pattern is assumed.
- Material properties are temperature-dependent.
- Natural convection due to gravity is accounted for.
- The Lorentz force is time – averaged over one oscillation period.
- Modelling of the solid-liquid phase transformation by an enthalpy-porosity approach [11] using a solidification range of the material.
- Inductive heating is neglected due to the strong heating of the laser source up to evaporation temperature of the metal.

B. Governing equations

In this paragraph, the governing equations for the mass conservation, momentum as well as energy transport are presented, see [12]:

- Mass Conservation

$$\nabla \cdot (\rho \boldsymbol{u}) = 0 \tag{1}$$

- Momentum equation

$$\rho(\boldsymbol{u} \cdot \nabla)\boldsymbol{u} = -\nabla p + \nabla \cdot \left(\eta\left(\nabla \boldsymbol{u} + (\nabla \boldsymbol{u})^T\right) - \frac{2}{3}\eta(\nabla \cdot \boldsymbol{u})\boldsymbol{I} \right) + \boldsymbol{F} \tag{2}$$

with source term

$$\boldsymbol{F} = -\rho \boldsymbol{g} - c_1 \frac{(1 - f_L)^2}{f_L^{\,3} + \varepsilon}(\boldsymbol{u} - \boldsymbol{u}_{weld}) + \langle \boldsymbol{j} \times \boldsymbol{B} \rangle \tag{3}$$

- Energy conservation

$$\rho C_p^{eff}\, \boldsymbol{u} \cdot \nabla T = \nabla \cdot (\lambda \nabla T) \tag{4}$$

Here, $\rho, \boldsymbol{u}, p, \eta, \boldsymbol{I}, \boldsymbol{g}, C_p^{eff}, T$ and λ are mass density, fluid velocity, pressure, dynamic viscosity, identity matrix, gravitational constant $\boldsymbol{g} = (0, 0, 9.81\ \mathrm{m/s^2})$, heat capacity, temperature and heat conductivity.

The latent heat of fusion was modeled by an effective heat capacity formulation

$$C_p^{eff} = C_p^0 + \frac{\exp\left[\left(\frac{T - T_{melt}}{\delta T}\right)^2\right]}{\sqrt{\pi}\,\delta T} H_f, \tag{5}$$

where C_p^0 is the heat capacity without latent heat and H_f is the latent heat amount being normalized around the melting temperature with a half width δT = 50 K.

The first source term on the right-hand side of (3) is the influence of gravity. The second term refers to the enthalpy-porosity approach to numerically handle the solidification around the melting temperature of the material. Therefore, an artificial range for melting and solidification called mushy zone is introduced, where f_L denotes the liquid fraction:

$$f_L = \begin{cases} 0 & T < T_{sol} \\ \dfrac{T - T_{sol}}{T_{sol} - T_{liq}} & T_{sol} \le T \le T_{liq} \\ 1 & T > T_{liq} \end{cases}. \tag{6}$$

In (3) c_1 and ε are constants, where the first is rather large and the latter is intended to avoid division by zero. The half interval between the liquidus and solidus temperature was chosen to be 3 K. The last term in (3) is the time-averaged Lorentz force that accounts for the coupling of the hydrodynamics with the electromagnetic field. It forms due to the alternating magnetic field and its induced eddy currents as well as the velocity-induced currents in the specimen. The Maxwell equations in quasi-stationary form for the magnetic field $\boldsymbol{B}$ and the electric field $\boldsymbol{E}$ are as follows:

$$\nabla \times \boldsymbol{B} = \mu_0 \boldsymbol{j}, \tag{7}$$

$$\nabla \times \boldsymbol{E} = -\frac{\partial \boldsymbol{B}}{\partial t}. \tag{8}$$

The generalized Ohms law in the case of moving electrically conducting fluid in a magnetic field reads:

$$\boldsymbol{j} = \sigma(\boldsymbol{E} + \boldsymbol{u} \times \boldsymbol{B}). \tag{9}$$

Hereby, the electromagnetic fields are coupled with the velocity field. $\boldsymbol{j}$ is the electric current density and σ the electric conductivity. A further significant aspect is the Hartmann effect. In the region within the penetration depth of the electromagnetic field, there is a contribution to the current density that comes from the movement of the conducting liquid metal in the magnetic field, note the last term in (9).

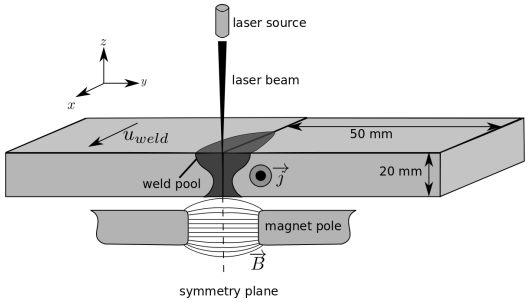

Fig. 1: Simulation domain.

That contribution to the current density results in a brake force that tends to weaken the liquid metal velocity. One can imagine this effect as a virtual contribution to the viscosity, which can be expressed as the ratio of magnetic induced to viscous drag in terms of the Hartmann number [7]

$$\mathrm{Ha}^2 = (B_{rms} L)^2 \frac{\sigma}{\eta}, \tag{10}$$

where L is the weld pool half width.
For an optimal compensation the penetration of the magnetic field should be around half the penetration depth of the laser. For the investigated aluminum specimen with 20 mm thickness, a frequency of 450 Hz was chosen corresponding to a magnetic field penetration of around 11 mm in the liquid metal. The skin depth δ for the electromagnetic field reads as follows [7]:

$$\delta = (\pi f \mu_0 \sigma)^{-1/2}, \tag{11}$$

where f is the frequency and μ_0 is the magnetic permeability of vacuum. Due to the fact that the frequency of potentially unstable surface waves are of lower order of magnitude than the excitation frequency of the magnetic field, it is feasible to use the time-averaged Lorentz force contribution thus avoiding the need for a time-consuming and memory-expensive calculation process. The applied oscillating electromagnetic field builds up a Lorentz force distribution that is mainly directed upwards in the melt. Therefore, this force counteracts the forces that are resulting from gravity. The corresponding Lorentz force contribution $\langle F_L^z \rangle$ integrated along a vertical axis in the melt leads to the magnetic pressure p_{EM} which is proportional to the effective value of the applied magnetic flux density squared:

$$p_{EM} = \int_z \langle F_L^z \rangle dz \propto \frac{B_{rms}^2}{2\mu_0}. \tag{12}$$

C. Boundary Conditions

The simulation domain for the metal flow problem using half-symmetry is 115 mm x 50 mm x 20 mm, note Fig. 1. The material parameters for the simulation can be seen in Fig. 2 and TABLE I, respectively. The cross section of the magnet poles as well as the distance between them was 25 mm. The magnet was located 2 mm below the weld specimen. The keyhole geometry is a right-circular cone with radius 0.4 mm at the upper side and 0.2 mm at the root side. The surface of the keyhole is fixed and the temperature is set to evaporation temperature. Flow normal to the keyhole walls is not allowed. Their surfaces are subjected to a slip condition.

The process velocity for the welding was set to 0.5 m/min. This value was experimentally determined to obtain full-penetration welding at 20 mm aluminum alloy plates.

TABLE I
MATERIAL PROPERTIES AT MELTING TEMPERATURE [13], [14]

Material property	Value	Unit
Melting temperature T_{melt}	933	K
Evaporation temperature T_{evap}	2700	K
Mass density ρ	2380	kg/m^3
Heat capacity C_p^{eff}	1180	J/kg K
Latent heat of fusion H_f	$3.97 \cdot 10^5$	J/kg
Thermal conductivity λ	91	W/m K
Dynamic viscosity η	$1.1 \cdot 10^{-3}$	Pa s
Marangoni coefficient $\partial\gamma/\partial T$	$-1.55 \cdot 10^{-4}$	N/m K
Electric conductivity σ	$4 \cdot 10^6$	S/m

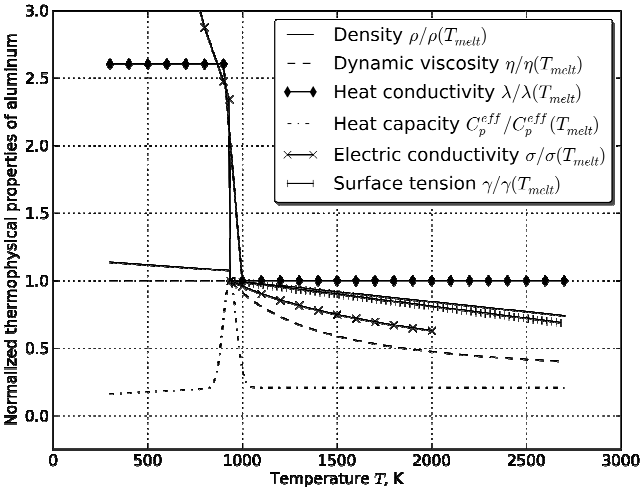

Fig. 2: Normalized thermophysical properties of aluminum.

At the upper and lower surfaces, Marangoni stresses were applied with $\boldsymbol{u} = (u, v, w)$:

$$\eta \frac{\partial u}{\partial z} = -\frac{\partial \gamma}{\partial T} \frac{\partial T}{\partial x}, \tag{13}$$

$$\eta \frac{\partial v}{\partial z} = -\frac{\partial \gamma}{\partial T} \frac{\partial T}{\partial y}. \tag{14}$$

These conditions result from the temperature dependence of the surface tension γ. The upper and lower walls are adiabatic and are subjected to a slip condition as well. At the front side of the specimen, the temperature is set to room. The symmetry plane is adiabatic as well and there are only tangential components of the velocity allowed.

ISBN: 978-1-61804-020-6

III. Results & Discussion

In this paper, the influence of the interaction between fluid flow of molten metal, heat transfer and electromagnetic Lorentz force contribution was numerically investigated. It was found that a magnetic flux density of around 80 mT is enough to fully compensate the hydrostatic pressure caused by the action of gravity, see Fig. 4. The gray area marks the hydrostatic pressure at the melting and evaporation temperature, respectively. At the weld pool surfaces, the resulting net hydrostatic pressure will be in between these values.

Without the electromagnetic support system, the surface tension at the lower boundary cannot balance the hydrostatic pressure of the molten metal and drops out consequently, see the root side of a 20 mm thick weld of aluminum alloy 5754 in Fig. 5. Note the difference between the weld on the left side, where the magnet system was disabled and the right side with electromagnetic support system enabled. See also the cross section of the right weld which is shown in Fig. 6.
Here, it is clear, that the molten metal was moved upwards by the Lorentz forces. Note the slight overcompensation of the sagging at the root side of the weld.

In Fig. 3, the weld pool symmetry plane is shown in the reference case without electromagnetic support system, where the Marangoni vortices at the lower and upper surfaces due to the applied Marangoni stresses occur (see (13) and (14)). Also note the natural convection influence near the keyhole cavity. There, the density is lower than in the surrounding area leading to lower gravitational forces. Therefore, the hot liquid metal flows up and comes to the region of influence of the upper vortex formation. The hot liquid metal is then accelerated along the upper surface and, accounting for mass conservation, comes back at some mm below the surface. The interaction of the natural convection with the Marangoni vortex leads to a larger weld pool at the upper surface.

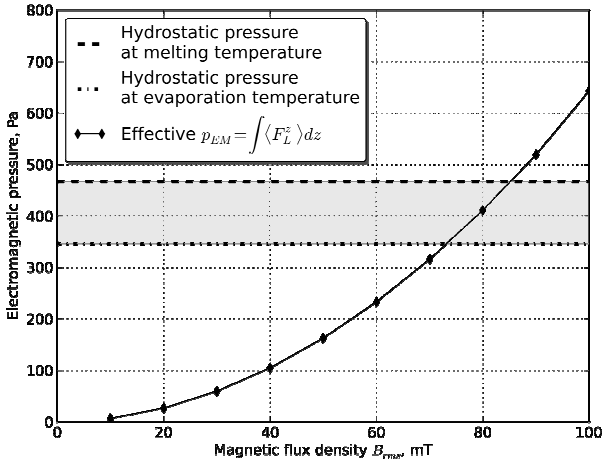

Fig. 4: Magnetic pressure for increasing magnetic flux density.

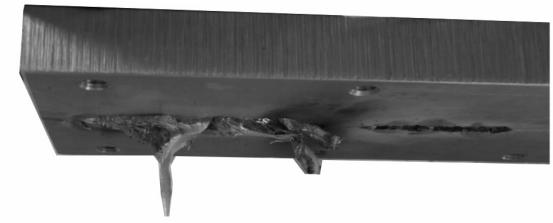

Fig. 5: Root side of a 20 mm thick welded aluminum alloy 5754 without (left) and with electromagnetic support system (right).

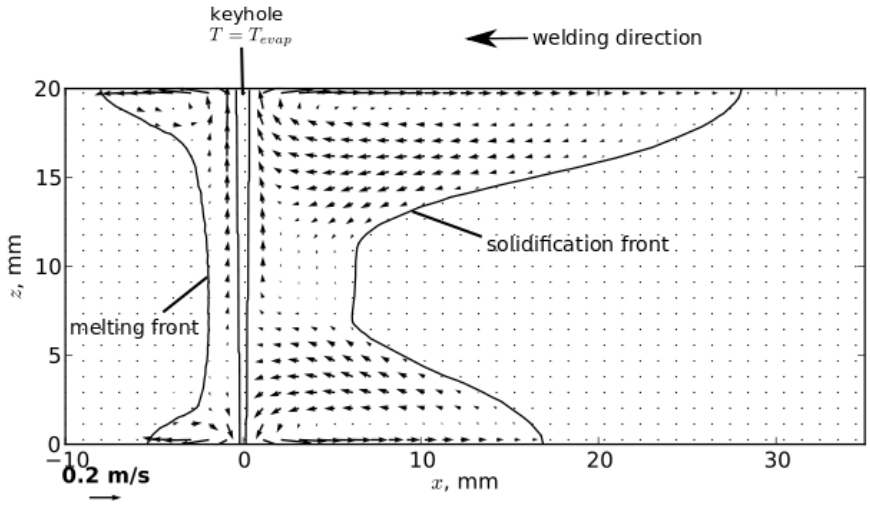

Fig. 3: Symmetry section in the reference case without magnetic support system. Solid lines represent the evaporation and the melting isotherm, respectively. Arrows denote the liquid metal velocity.

ISBN: 978-1-61804-020-6

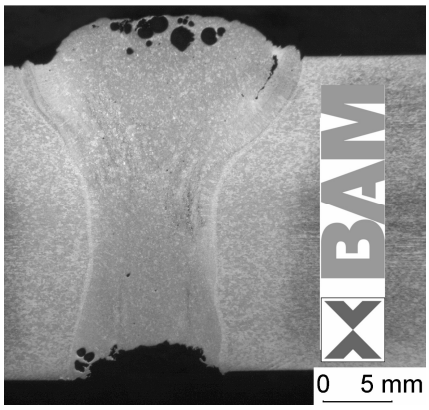

Fig. 6: Cross section of a 20 mm thick weld of 5754 aluminum alloy with welding speed 0.5 m/min at 15 kW laser power in flat position. The electromagnetic excitation frequency was chosen to be 459 Hz at B_{rms} = 77 mT.

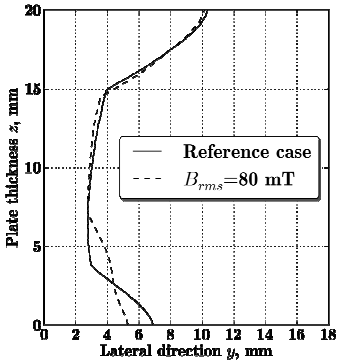

Fig. 8: Fusion zone from computer simulations with and without application of electromagnetic fields.

In Fig. 7, the same plane is shown with magnet field support system applied. The reference value of the magnetic flux density was set to 80 mT. It is remarkable, that the flow pattern completely changed by the influence of the Lorentz force distribution in the melt. Compared to the reference case in Fig. 3, the area that is influenced by the vortex on the lower side where the magnet system is located is larger in vertical direction. Note the intense vortex at the trailing side of the keyhole. This vortex is directed in the same direction as the Marangoni vortex in the reference case and is also supported by a rotational component of the Lorentz force distribution that comes from the temperature-dependence of the electric conductivity, see Fig. 2. This flow system interferes with the flow that results from the upwards directed potential part of the Lorentz force, which acts as a pressure. The upper part of the weld pool is similar to the reference configuration resulting from the applied oscillation frequency of the magnetic field and its according limited penetration depth.

In the lower region the magnetic induced drag is larger than the viscous one, corresponding to a Hartmann number around 500, see (10). Hereby, the weld pool cross section in Fig. 7 is heavily influenced.

IV. Conclusion

The influence of the application of a harmonic magnetic field on the laser welding of a 20 mm thick aluminum plate was numerically investigated using the finite element software COMSOL Multiphysics. Fluid velocity, pressure, temperature as well as electromagnetic field quantities were calculated.

It was shown, that the magnetic pressure that is mainly resulting from the applied ac magnetic field and its eddy currents in the specimen is able to compensate for the hydrostatic pressure of the column of liquid aluminum above.

Moreover the magnetic induced drag lowers the influence of the Marangoni stresses at the side of the specimen where the magnet system is located.

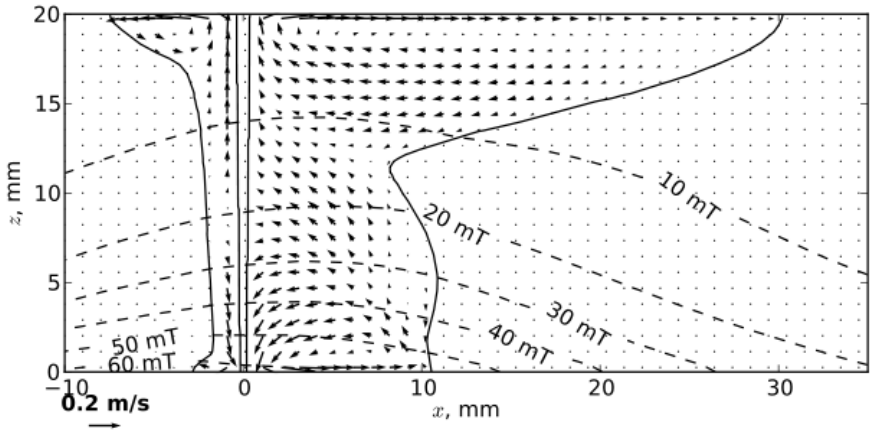

Fig. 7: Symmetry section in the reference case with magnetic support system applied. Solid lines represent the evaporation and the melting isotherm, respectively. Arrows denote the liquid metal velocity.

ISBN: 978-1-61804-020-6

REFERENCES

[1] Rethmeier M, Gook S, Lammers M and Gumenyuk A Laser-Hybrid Welding of Thick Plates up to 32 mm using a 20 kW Fibre Laser 2009 *Japan Welding Society* **27** 74s – 79s.

[2] Ready J F and Farson D F 2001 *LIA Handbook of Laser Materials Processing* Springer, Berlin.

[3] Dowden J 2009 *The Theory of Laser Materials Processing: Heat and Mass Transfer in Modern Technology* Springer Netherlands.

[4] Fuhrich T, Berger P and Hügel H 2001 Marangoni effect in laser deep penetration welding of steel *J. Laser Appl.* **13** 178 – 86.

[5] Mahrle A and Schmidt J 2002 The influence of fluid flow phenomena on the laser beam welding process *Int. J. Heat Fluid Fl.* **23** 288 – 97.

[6] Ribic B, Rai R and DebRoy T 2008 Numerical simulation of heat transfer and fluid flow in GTA/laser hybrid welding *Sci. Technol. Weld. Joi.* **13** 683 – 93.

[7] Moreau R 1990 *Magnetohydrodynamics* Kluwer Academic Publishers.

[8] Bojarevics V, Freibergs J A, Shilova E I and Shcherbinin E V 1989 *Electrically induced vertical flows* Kluwer London.

[9] Avilov V V, Moldovan R, Berger P and Graf T 2008 Electromagnetic weld pool control system for laser beam welding of thick metal plates *Proceedings of the IWOTE08 BIAS Verlag Bremen.* 413 – 20.

[10] Avilov V V, Moldovan R, Berger P, Graf T and Mock D 2009 Electromagnetic weld pool control by CO2 and YAG disk laser welding of thick stainless steel plates *Proceedings of EPM 2009 Dresden Germany.*

[11] Brent A D, Voller V R and Reid K J 1998 Enthalpy-porosity technique for modelling convection-diffusion phase change: application to the melting of pure metal *Numer. Heat Transfer* **13** 297 – 318.

[12] COMSOL *CFD Module User's Guide* Version 4.1 October 2010.

[13] Mills K C 2002 *Recommended Values of Thermophysical Properties for Selected Commercial Alloys* Woodhead Publishing Ltd.

[14] Keene B J 1993 Review of data for the surface tension of pure metals *Int. Mater. Rev.* **38** 157 – 92.

ISBN: 978-1-61804-020-6